Distribution of nearest distances between nodal points for the Berry function in two dimensions

Alexander I. Saichev,[1,2] Karl-Fredrik Berggren,[2] and Almas F. Sadreev[2,3]
[1]*Department of Radiophysics, Nizhny Novgorod University, Gagarin prospekt 23, 603600 Nizhny Novgorod, Russia*
[2]*Department of Physics and Measurement Technology, Linköping University, S-581 83 Linköping, Sweden*
[3]*Kirensky Institute of Physics, 660036, Krasnoyarsk, Russia*
(Received 31 October 2000; revised manuscript received 11 April 2001; published 29 August 2001)

According to Berry a wave-chaotic state may be viewed as a superposition of monochromatic plane waves with random phases and amplitudes. Here we consider the distribution of nodal points associated with this state. Using the property that both the real and imaginary parts of the wave function are random Gaussian fields we analyze the correlation function and densities of the nodal points. Using two approaches (the Poisson and Bernoulli) we derive the distribution of nearest neighbor separations. Furthermore the distribution functions for nodal points with specific chirality are found. Comparison is made with results from numerical calculations for the Berry wave function.

DOI: 10.1103/PhysRevE.64.036222 PACS number(s): 05.45.Mt, 02.50.Cw, 03.65.Ta

I. INTRODUCTION

The nature of the quantum eigenstates in billiards, which are classically chaotic, has been subject to much theoretical and experimental work. The seminal studies by McDonald and Kaufmann [1] of the morphology of the two-dimensional (2D) eigenstates in a closed Bunimovich stadium have revealed characteristic complex patterns of disordered, undirectional and noncrossing nodal lines. The spatial behavior of the eigenstates of chaotic billiards is still of considerable theoretical and experimental interest. For recent theory see, e.g., Refs. [2–5], and references cited therein; examples of measurements on electron billiards and wave-dynamical analogs are found in Ref. [6]. Other well known signatures of quantum chaos in closed billiards are related to the distribution of nearest level separations and spectral rigidity.

For open billiards, i.e., billiards with attached leads, the picture is less clear. One may use the poles of the scattering matrix that are related to the decay time from a billiard [7–9]. When transport through a billiard takes place one may as an alternative focus on the fact that the wave function ψ is a scattering state with both real and imaginary parts. If we restrict ourselves to 2D systems, as we will do throughout this work, this means that there are two separate sets of nodal lines at which either $\mathrm{Re}[\psi]$ or $\mathrm{Im}[\psi]$ vanish. The intersections of the two sets at which $\mathrm{Re}[\psi]=\mathrm{Im}[\psi]=0$ define the nodal points. Numerical simulations have shown that the shape of distribution function for the nearest distances between these nodal points (DFNDNP) depends on whether the billiard is nominally either regular or irregular [10]. For transmission through chaotic billiards the DFNDNP appears to have a general characteristic form, while for regular billiards like, for example, rectangular ones there are specific features of the DFNDNP that depend on the particular geometry, at least as long as only a few channels are open. Thus, besides the vivid physical role played by the nodal points as centers of vortical motion [11–17], their statistical distribution may tell if chaos is present or not. The present work relates to quantum transport in open electron billiards. The issue of wave function singularities is, however, part a much broader context [18–22].

An appealing argument that favors our view that DFNDNP serves as a signature of quantum chaos is the coincidence with the corresponding distribution function for the Berry state [10]. According to Berry's conjecture a chaotic state can be viewed as a superposition of a large number of interfering monochromatic de Broglie waves [18]

$$\psi(\mathbf{r})=\sum_j a_j \exp(i\mathbf{k}_j\cdot\mathbf{r}+\phi_j), \tag{1}$$

where a_j and ϕ_j are independent random variables and $\mathbf{k}_j$ are randomly oriented wave vectors of equal length. The Berry wave function may be regarded as a standard measure of quantum chaos. In fact, there are beautiful experimental observations of Berry waves on the surface of water in an agitated ripple tank with stadium-shaped walls [23].

So far all our conclusions about DFNDNP rest on numerical experiments [10]. The Berry state is, however, available in a mathematical form that invites to analytic approaches. In the present work we will therefore model the DFNDNP $f(r)$ and its main asymptotic behavior analytically using the fundamental property that the Berry function (1) is Gaussian random field [18]. We will also show that there are other types of distribution functions that are related to the chirality of the nodal points. Each nodal point is a topological singularity of the wave function [12,13,15–18]. As a result there is a vortex centered around each nodal point with definite chirality depending on whether the current flows clockwise or counterclockwise as indicated in Fig. 1. We therefore label each nodal point by $\sigma=\pm 1$. In analogy with $f(r)$ we therefore introduce the distribution functions $f_{\sigma,\sigma'}(r)$ for nearest neighbor separations between points with chiralities σ and σ'. Analytic expressions for these distributions will be derived below and compared with numerical computations using the Berry wave function. As will be pointed out in the text our results partly overlap with recent work by Berry and Dennis [18] (the pair correlation functions $g_{\sigma,\sigma'}$ and the relation between the mean density and wave number k). Most recently Dennis has also considered the distribution of nearest distances among nodal points using the Poisson model [24]. The statistical mechanics of topological defects have also been discussed by Halperin [25].

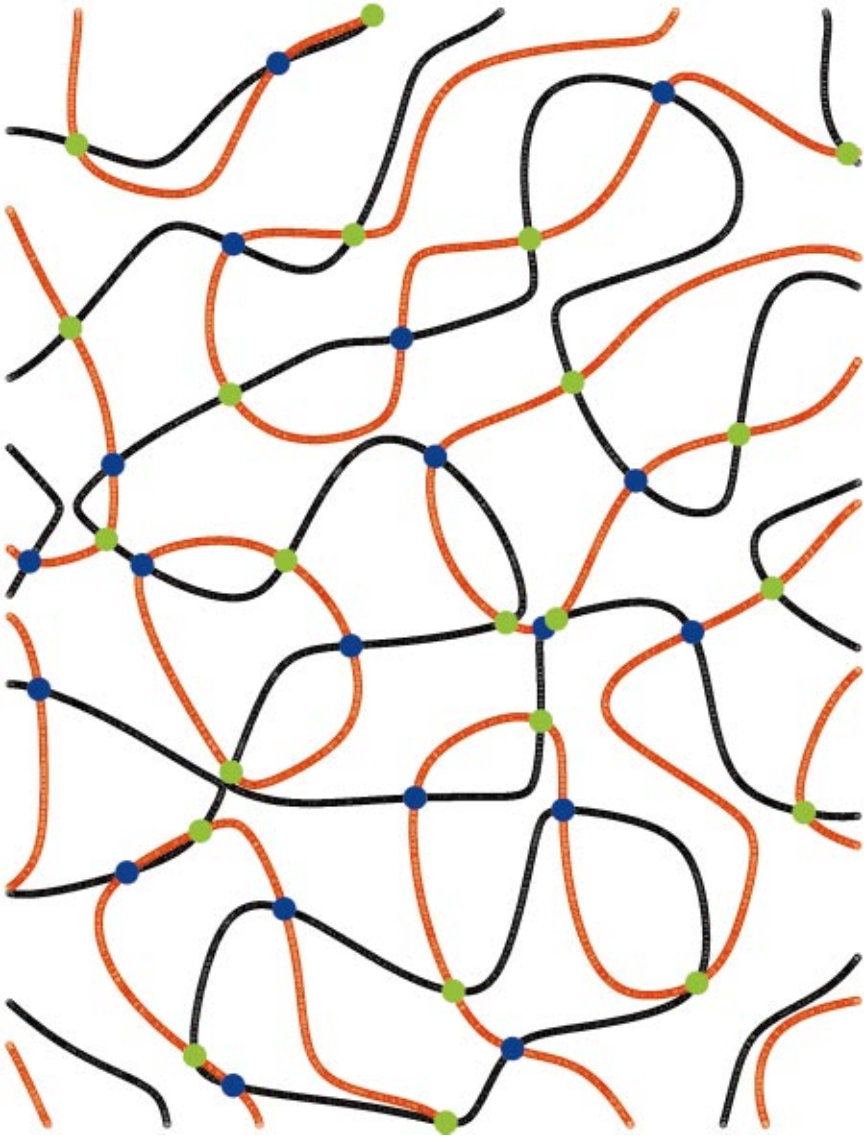

FIG. 1. (Color) Typical pattern of nodal lines $\mathrm{Im}[\psi(x,y)]=0$ and $\mathrm{Re}[\psi(x,y)]=0$ for the Berry function in the (x, y) plane. Nodal lines in each set do not cross. Points at which the two sets intersect are the nodal points around which there is vortical flow in either clockwise or counterclockwise direction.

In the following sections we will derive expressions for the distributions of nearest neighbor separations between points with chiralities σ and σ'. For this purpose we will also have to consider the pair correlation functions $g_{\sigma,\sigma'}$. We will make use of two different analytic approaches based on the Poisson and Bernoulli models. In addition we will also calculate the distributions by direct numerical methods, i.e., we locate the nodal points by simply computing the nodal lines for $\mathrm{Im}(\Psi)$ and $\mathrm{Re}(\Psi)$ and how they cross. In principle the numerical results represent the correct distributions and gives us a way to test the accuracy of the different analytic approaches.

II. DEFINITION OF VARIABLES

Consider the Berry function (1) as the complex random function

$$\psi(\mathbf{r})=u(\mathbf{r})+v(\mathbf{r}), \tag{2}$$

where $\mathbf{r}$ is the 2D position with Cartesian coordinates xy and $u(\mathbf{r}),v(\mathbf{r})$ are two real random fields. We assume that $u(\mathbf{r})$ and $v(\mathbf{r})$ are mutually statistically independent, homogeneous and isotropic Gaussian random fields with zero mean. The correlation function has the well known form

$$a(s)=\langle u(\mathbf{r})u(\mathbf{r}+\mathbf{s})\rangle=\langle v(\mathbf{r})v(\mathbf{r}+\mathbf{s})\rangle=J_0(ks), \tag{3}$$

where $s=|\mathbf{s}|$ and $k=|\mathbf{k}|$. This result is a direct consequence of the Berry function (1). To find the statistical properties of the nodal points $\mathbf{r}_j$ we have to consider the intersections of the zero level curves (nodal lines) of the fields $u(\mathbf{r})$ and $v(\mathbf{r})$, i.e., the roots of the two equations:

$$u(\mathbf{r}_j)=v(\mathbf{r}_j)=0 \quad (\mathbf{r}_j\in\mathbb{R}^2).$$

As mentioned in the Introduction the nodal points are the centers of vortices. The associated probability current $\mathbf{J}(\mathbf{r})$ is proportional to

$$\mathbf{J}(\mathbf{r})=\mathrm{Re}[\psi^*(\mathbf{r})i\nabla\psi(\mathbf{r})]=v(\mathbf{r})\nabla u(\mathbf{r})-u(\mathbf{r})\nabla v(\mathbf{r}). \tag{4}$$

In the present work we consider the vorticity field

$$\boldsymbol{\omega} = \boldsymbol{\nabla} \times \mathbf{J}. \tag{5}$$

In our two-dimensional case it is normal to the (x, y) plane, i.e., $\boldsymbol{\omega}(\mathbf{r}) = \omega(\mathbf{r})\hat{\mathbf{n}}_z$ where $\hat{\mathbf{n}}_z$ is the normal unit vector. Substituting Eq. (4) into Eq. (5) we have

$$\boldsymbol{\omega}(\mathbf{r}) = [\boldsymbol{\nabla} u(\mathbf{r}) \times \boldsymbol{\nabla} v(\mathbf{r})]. \tag{6}$$

At the nodal point $\mathbf{r}_j$

$$\omega_j = \omega(\mathbf{r}_j)$$

is the angular velocity of the current in the very vicinity of $\mathbf{r}_j$. In the following we will call ω_j the *vorticity* of the jth nodal point.

The nodal points are topological singularities of the complex function (2) because they are responsible for the vortices. This means that when the following loop integral encloses a nodal point one has [11,12,15–17]

$$\oint \boldsymbol{\nabla} \theta d\mathbf{r} = \pm 2\pi, \tag{7}$$

where θ is the phase of the wave function. In what follows we use the definition

$$\sigma_j = \frac{\omega_j}{|\omega_j|} \tag{8}$$

for which σ_j takes the values ± 1 for clockwise and counterclockwise vorticities ω_j, respectively. Therefore Eq. (8) defines the sign of the vorticity of the nodal points. Below we will refer to σ as chirality. Alternatively it is named topological charge [18] or winding number [25]. There are as many points with $\sigma = 1$ as with $\sigma = -1$. Sum rules for points of this kind were established by Longuet-Higgins long ago [26,27].

III. GENERAL FORMULAS FOR THE DENSITY OF NODAL POINTS

If we introduce the density of nodal points as

$$\mathcal{R}(\mathbf{r}) = |\boldsymbol{\omega}(\mathbf{r}_j)| \, \delta(u(\mathbf{r})) \delta(v(\mathbf{r})) \tag{9}$$

we obtain

$$\mathcal{R}(\mathbf{r}) = \sum_j \delta(\mathbf{r} - \mathbf{r}_j). \tag{10}$$

For later reference let us also introduce the singular function

$$\mathcal{R}_v(\mathbf{r}) = \omega(\mathbf{r}) \, \delta(u(\mathbf{r})) \delta(v(\mathbf{r})) = \sum_j \sigma_j \delta(\mathbf{r} - \mathbf{r}_j). \tag{11}$$

Next, let us define the mean density

$$\langle \mathcal{R}(\mathbf{r}) \rangle = \rho \tag{12}$$

and the correlation function for the random density

$$G(s) = \langle \mathcal{R}(\mathbf{r}) \mathcal{R}(\mathbf{r} - \mathbf{s}) \rangle = \left\langle \sum_{i,j} \delta(\mathbf{r} - \mathbf{r}_i) \delta(\mathbf{r} - \mathbf{r}_j - \mathbf{s}) \right\rangle. \tag{13}$$

Notice that because $\mathcal{R}(\mathbf{r})$ is a statistically homogeneous and isotropic random field, the mean density ρ is constant and the correlation function $G(s)$ depends only on the distance s between the points of observation $\mathbf{r}$ and $\mathbf{r} - \mathbf{s}$. Formulas (9), (11), (12) and (13) form the basis of the statistical analysis of the nodal points distribution assuming that the functions $u(\mathbf{r})$ and $v(\mathbf{r})$ are random functions.

The mean density defines a characteristic scale

$$s_\rho = \frac{1}{\sqrt{\rho}}, \tag{14}$$

which we will use below as the natural unit of distances in the ''gas'' of randomly distributed points, i.e., we will use the dimensionless variable

$$\ell = \frac{s}{s_\rho} = \sqrt{\rho} s. \tag{15}$$

Moreover it is convenient to formulate some analytical results in terms of the dimensionless pair-pair correlation function with dimensionless argument.

$$g(\ell) = \frac{1}{\rho^2} G\left(\frac{\ell}{\sqrt{\rho}} \right). \tag{16}$$

We now introduce the mean density $\gamma(r)$ around a given point. One can show that

$$\gamma(s) = \frac{1}{\rho} G(s), \tag{17}$$

which will play a crucial role in the following derivation of DFNDNP for the Berry function.

We now consider some useful relations for the statistics of the nodal points. First, consider the mean number of points inside a circle C_r with radius r centered at some given point. It is obvious that the mean number of points enclosed by the circle is equal to

$$\langle n(r) \rangle = 2\pi \int_0^r \gamma(y) y dy. \tag{18}$$

Using the dimensionless coordinate (15) one obtains

$$\langle n(\ell) \rangle = 2\pi \int_0^\ell g(r) r dr. \tag{19}$$

This relation takes into account that the dimensionless correlation function $g(r)$ is at the same time the dimensionless mean density. Second, consider also the relation for the mean number of nodal points

$$\langle n(\ell) \rangle = \sum_{n=1}^{\infty} n P(n; \ell).$$

Here $P(n;\ell)$ is the probability that n neighboring points belong to the circle. These probabilities satisfy the normalization condition

$$P(0;\ell)=1-\sum_{n=1}^{\infty} P(n;\ell). \tag{20}$$

The probability $P(0;\ell)$ is of great importance because it is directly related to the distribution function for nearest distances between a given point and its neighboring points (DFNDNP) $f_{\min}(\ell)$. This is because the cumulative distribution of the nearest distances $\ell_{\min}$ is given by

$$F_{\min}(\ell)=P(\ell_{\min}<\ell)=1-P(0;\ell). \tag{21}$$

Therefore we may now write the following relation for the dimensionless distribution of nearest distances

$$f_{\min}(\ell)=-\frac{\partial}{\partial \ell}P(0;\ell). \tag{22}$$

Thus, the last formula reduces the problem of calculating the DFNDNP to that of finding $P(0;\ell)$. Below we will find approximate expressions for $P(0;\ell)$. However, we will first present asymptotic formulas for $P(0;\ell)$ and the DFNDNP. We assume that $P(n;\ell)$ is a well-behaved function. For small ℓ one may therefore replace the exact relations (19) and (20) with the asymptotic forms

$$\langle n(\ell)\rangle \sim P(1;\ell), \quad P(0;\ell)\sim 1-P(1;\ell), \quad \ell\to 0.$$

Finally, from Eqs. (19) and (22) and the last relation above one obtains the following asymptotic formula for the exact DFNDNP

$$f_{\min}(\ell)\sim \frac{\partial}{\partial \ell}\langle n(\ell)\rangle = 2\pi \ell g(\ell) \quad (\ell\to 0). \tag{23}$$

Let us now apply these general considerations to the Berry function (1). First of all we will calculate the mean density ρ in Eq. (12). Using the definition (9) and the fact that the variables of the homogeneous Gaussian field and its derivatives are statistically independent at the same point we have

$$\rho=\langle|\omega(\mathbf{r})|\rangle\langle\delta(u(\mathbf{r}))\rangle\langle\delta(u(\mathbf{r}))\rangle. \tag{24}$$

It is straightforward to show that

$$\langle\delta(u(\mathbf{r}))\rangle\langle\delta(v(\mathbf{r}))\rangle=\frac{1}{2\pi}, \quad \langle|\omega|\rangle=\frac{k^2}{2}, \tag{25}$$

where k is modulus of wave vector of the Berry function (1). Therefore, substituting Eq. (25) into Eq. (24) we obtain the final expression for the mean density

$$\rho=\frac{k^2}{4\pi}. \tag{26}$$

This exact relation has been derived recently also by Berry and Dennis [18]. A more general expression for ρ has been derived by Halperin [25].

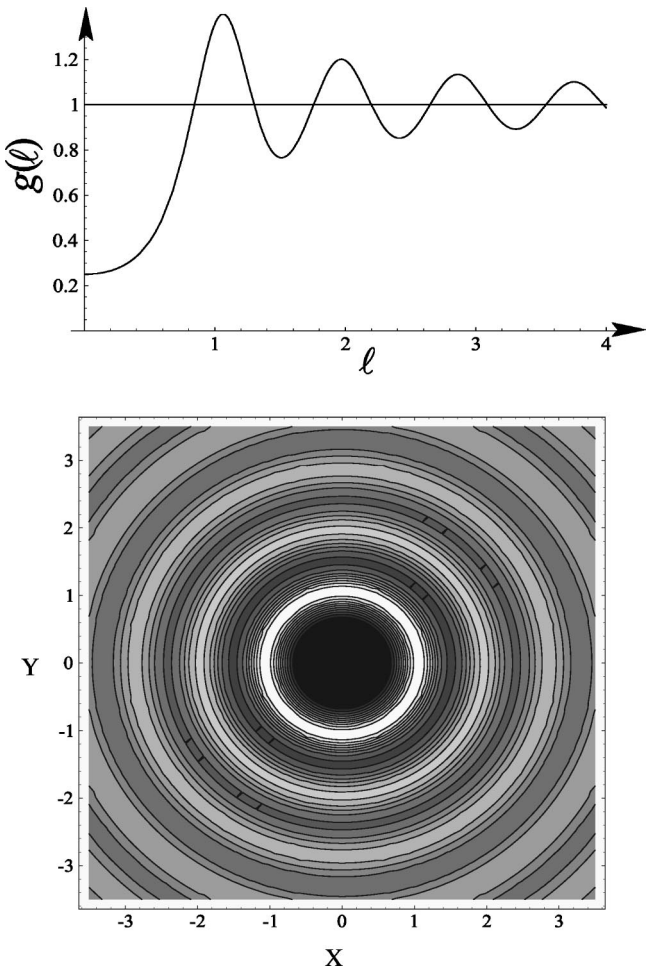

FIG. 2. The dimensionless correlation function g nodal for the Berry wave function (1) versus the dimensionless radius ℓ. The lower frame displays the same function in the (x, y) plane (x and y dimensionless).

Second, consider the density correlation function (13)

$$G(s)=\langle|\omega(\mathbf{r})\omega(\mathbf{r}+\mathbf{s})|\,\delta(u(\mathbf{r}))\delta(u(\mathbf{r}+\mathbf{s}))\times\delta(v(\mathbf{r}))\delta(v(\mathbf{r}+\mathbf{s}))\rangle. \tag{27}$$

The calculation of $G(s)$ is given in the Appendix (A11) and the dimensionless pair correlation function for arbitrary ℓ is plotted in Fig. 2. The general behavior reminds superficially of the correlation functions for amorphous solids with short-range order and distinct shell-like structures present [28]. The correlations are, however, more long range in the present case. The same pair correlation function was recently obtained by Berry and Dennis [18], although expressed in a different analytic form. The derivations are somewhat tedious as indicated by the Appendix. It is therefore rewarding that there is perfect numerical agreement with Berry and Dennis' results [18]. Halperin [25] has given a general expression for the correlation function for topological defects. Insertion of Eq. (3) in his general expression yields results that deviate substantially from ours and Berry and Dennis' for small distances less than about the mean distance between the defects.

Using the expressions in the Appendix we can find the asymptotic expression

$$g(\ell) \sim 1/4 \quad (\ell \to 0) \tag{28}$$

from which we obtain the asymptote for the DFNDNP (23) at small ℓ

$$f_{\min}(\ell) \sim \frac{\pi}{2}\ell \quad (\ell \to 0). \tag{29}$$

This exact result is useful for testing approximate analytical solutions and numerical simulation data.

IV. THE POISSON AND BERNOULLI APPROXIMATIONS FOR THE DFNDNP

In order to model the DFNDNP by analytic means we may in a first attempt use the Poisson approximation. This approach has been discussed recently also by Dennis [24]. The Poisson approximation implies that all points around a given one (which is located in center) are statistically independent, i.e., it neglects higher-order correlations. Therefore we have to take into account correlations only between the given point and its neighbors. These correlations can be incorporated using the mean density of points γ around the given point (17). According to the Poisson law the probability that no other points belong to circle with dimensionless radius ℓ is

$$P(0,\ell) = \exp(-\langle n(\ell)\rangle) = \exp\left[-2\pi\int_0^{\ell} z g(z)\,dz\right]. \tag{30}$$

Using the relation (22), we easily obtain the formula for the DFNDNP in the Poissonian approximation

$$f_{\min}(\ell) \approx 2\pi\ell g(\ell)\exp\left[-2\pi\int_0^{\ell} z g(z)\,dz\right]. \tag{31}$$

One notes that for small ℓ the asymptote of the approximate DFNDNP (31) coincides with exact one (29).

For the special case of uniformly distributed and completely random points ($g(\ell)=1$) we immediately obtain the well known result [29,30]

$$f_{\min}(\ell) = 2\pi\ell\,\exp(-\pi\ell^2). \tag{32}$$

For convenience we also introduce the new dimensionless radius

$$r = \ell/\langle\ell\rangle, \tag{33}$$

which refers to mean distance between nearest nodal points $\langle\ell\rangle$. The main asymptotic for the DFNDNP (29) then reads

$$f(r) \sim (\ell)^2\frac{\pi}{2}r = \nu r. \tag{34}$$

A comparison between Eqs. (31), (32) and the numerically calculated DFNDNP are given in Fig. 3. Obviously the simplest model with ($g(\ell)=1$) cannot reproduce the true

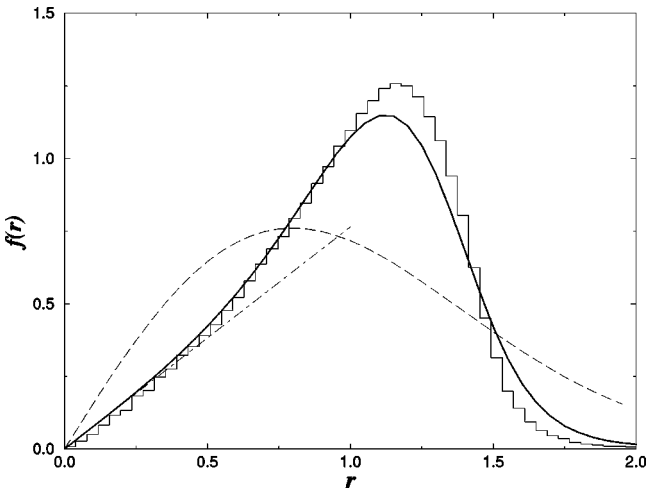

FIG. 3. DFNDNP versus dimensionless distance $r=\ell/\langle\ell\rangle$ for (a) random points (32) (dashed curve) and (b) for the Poissonian approximation (31) (solid curve) with $\langle\ell\rangle=0.657$. The straight dash-dot line is the corresponding asymptote (34). The histogram shows the distribution as obtained from direct numerical calculations of the positions of the nodal points $\mathrm{Re}(\psi(x_j,y_j)) = \mathrm{Im}(\psi(x_j,y_j))=0$ for the Berry function (1). In these simulations we have generated the nodal points in a large number of samples, typically of size (60×60) and with $k=\sqrt{2\pi}$. The number of random plane waves included has ranged from 20 to 80. In the example shown we have included 40 plane waves and averaged over 200 samples. Except for statistical variations the same results are obtained also for other choices of the number of plane waves, sample size, and value of k.

DFNDNP for the simple reason that the nodal points are not random points. The Poisson approximated function (31) is obviously in much better agreement with the numerical results although the distribution falls off too quickly at large separations. The agreement for small z is more satisfactory with $\nu=0.765$, which is rather close to the value 0.68 obtained from the direct numerical calculations. Although the Poissonian modeling gives reasonable results we need to go beyond it for a better description of the intrinsic statistical, higher-order correlations among the nodal points as indicated by Fig. 2.

A general disadvantage of the Poissonian approach is that all nodal points are competing with each other to be neighbors of a given point. It is clear, however, that only nearest neighbors of the given point actually participate in such a competition. Therefore we consider the Bernoulli approximation for the nearest distances of points that takes into account the competition between neighboring points. Similar to the Poisson approximation we again consider the circle $\mathcal{C}_{\mathcal{R}}$ of radius R with the center at a given point $\mathcal{O}$ and assume that all points except the given one are statistically independent. Furthermore, let us assume that the total number of points inside the circle $\mathcal{C}_{\mathcal{R}}$ is just equal to the mean density integral

$$n(R) = 2\pi\int_0^R g(\ell)\ell\,d\ell. \tag{35}$$

With these conditions the distribution of each randomly located point belonging to $\mathcal{C}_{\mathcal{R}}$ point is exactly equal to

$$f(\ell)=\frac{g(\ell)}{n(R)}. \tag{36}$$

Next, let us consider another circle $\mathcal{C}_\ell$ with the center at the same origin $\mathcal{O}$ and radius $\ell<R$. Obviously the probability to find a point in this smaller circle is equal to

$$p(\ell)=\int_{C_\ell} f(\ell)d^2\ell=\frac{\langle n(\ell)\rangle}{n(R)}, \tag{37}$$

where

$$\langle n(\ell)\rangle=2\pi\int_0^\ell g(r)rdr. \tag{38}$$

In the same way we have that the probability that a point does not fall into the circle $\mathcal{C}_\ell$ is equal to

$$q(\ell)=1-p(\ell)=1-\frac{\langle n(\ell)\rangle}{n(R)}. \tag{39}$$

Since points are statistically independent the probability for all points to be outside the circle C_ℓ equals

$$P(0;\ell)=\left(1-\frac{\langle n(\ell)\rangle}{n(R)}\right)^{n(R)}. \tag{40}$$

From Eqs. (21), (22), and (35) it follows directly that

$$f_{\min}(\ell)=\frac{\partial}{\partial\ell}P(0;\ell)=2\pi\ell g(\ell)\left(1-\frac{\langle n(\ell)\rangle}{n(R)}\right)^{n(R)-1}. \tag{41}$$

To obtain the DFNDNP analytically we make the following approaches within the Bernoulli approximation.

(i) In formula (41) we replace the number of points $n(R)$ by the mean number of points $\langle n(R)\rangle$ Eq. (38).

(ii) We choose the radius R in such a way that inside the circle C_R there are a certain number of points that compete with each other to be the nearest neighbor to $\mathcal{O}$. The minimum number of points in the circle is obviously three if we also include the central point.

In the following we will simply use this value. As a result we obtain, instead of formula (A10), the following expression:

$$f_{\min}(\ell)\cong 2\pi\ell g(\ell)\left(1-\frac{\langle(\ell)\rangle}{3}\right)^2. \tag{42}$$

It is easy to verify that this approximate distribution is normalized and has the same asymptote as the exact distribution function (29).

In Fig. 4 the analytic results in Eq. (42) are compared with the numerical distribution obtained directly from the Berry function. The Bernoulli approach is evidently more powerful than our previous attempt in predicting the DFNDNP (31). The reason would be that we now catch some of the higher-order correlations.

The distribution (42) has the same linear behavior at small

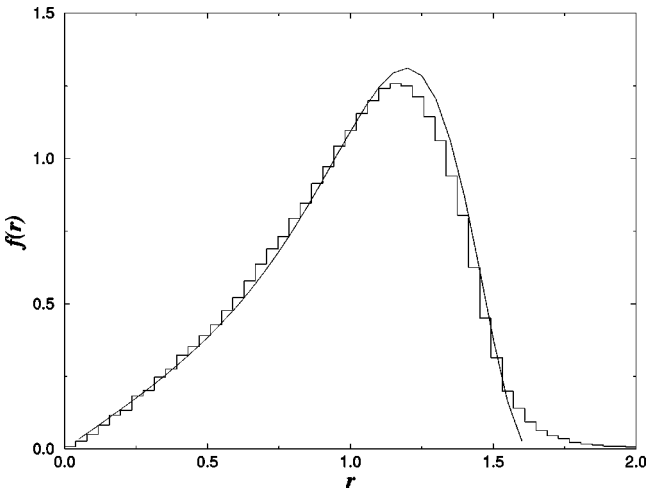

FIG. 4. Plots of the DFNDNP for the Berry function (1) versus dimensionless distance (33) with $\langle\ell\rangle=0.658$. Solid curve is the Bernoulli approximated distribution (42). The histogram is the same as in Fig. 3.

ℓ as in previous expressions (29) and (34). The coefficient $\nu=0.678$ that is quite close to numerics (0.68).

V. THE MEAN CHIRAL DENSITIES AND CORRELATION FUNCTIONS

To gain more detailed statistics of nodal points we consider the statistical characteristics of chiral-dependent nodal points density similar to Eq. (11)

$$\mathcal{R}_\sigma(\mathbf{r})=\sum_{j_\sigma}\delta(\mathbf{r}-\mathbf{r}_{j_\sigma}), \tag{43}$$

where j_σ numerates positions of vortices with chirality $\sigma=\pm1$. Formulas (10) and (11) can be written via the chiral densities (43)

$$\mathcal{R}_v(\mathbf{r})=\sum_\sigma\mathcal{R}_\sigma,\quad \mathcal{R}_v=\sum_\sigma\sigma\mathcal{R}_\sigma. \tag{44}$$

Similar to Eq. (12) we introduce the chiral mean densities

$$\langle\mathcal{R}_\sigma(\mathbf{r})\rangle=\rho_\sigma=\rho/2. \tag{45}$$

The last equality follows from the mean spatial isotropy of the Berry function (1), which implies that in mean there is no preferred chirality of nodal points.

Moreover we introduce the auxiliary chiral correlation function

$$G_v(s)=\langle\mathcal{R}_v(\mathbf{r})\mathcal{R}_v(\mathbf{r}-\mathbf{s})\rangle=\left\langle\sum_{i,j}\sigma_i\delta(\mathbf{r}-\mathbf{r}_i)\sigma_j\delta(\mathbf{r}-\mathbf{r}_j-\mathbf{s})\right\rangle \tag{46}$$

and correlation functions of the chiral mean densities (43)

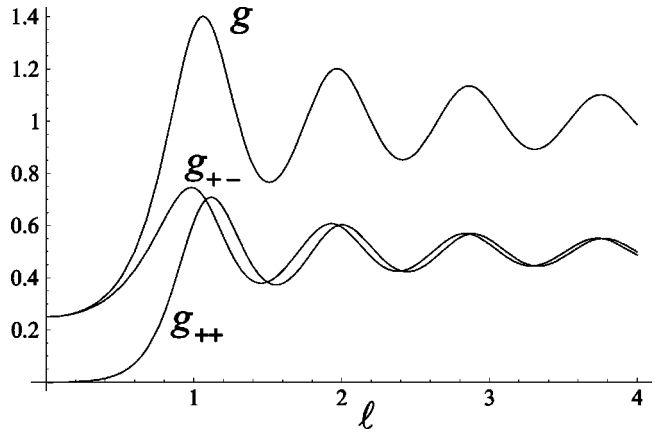

FIG. 5. Plots of the dimensionless correlation functions $g_{\sigma,\sigma}(\ell)=g_{++}$, $g_{\sigma,-\sigma}(\ell)=g_{+-}$, and $g(\ell)$ as defined in Eq. (51).

$$G_{\sigma,\sigma'}(s)=\langle \mathcal{R}_\sigma(\mathbf{r})\mathcal{R}_{\sigma'}(\mathbf{r}-\mathbf{s})\rangle = \left\langle \sum_{i_\sigma j'_\sigma} \delta(\mathbf{r}-\mathbf{r}_{i_\sigma})\,\delta(\mathbf{r}-\mathbf{r}_{j_{\sigma'}}-\mathbf{s}) \right\rangle. \tag{47}$$

From relations (10), (11), (13), (46), and (47) it follows that

$$G_{\sigma\sigma'}(s)=\tfrac{1}{4}[G(s)+\sigma\sigma' G_v(s)]. \tag{48}$$

Consider a nodal point with chirality σ. Similar to Eq. (17) we define the mean chiral densities around this point

$$\gamma_{\sigma\sigma'}(s)=\frac{2}{\rho}G_{\sigma\sigma'}(s). \tag{49}$$

Then from Eqs. (48) and (49) we obtain

$$\gamma_{\sigma\sigma'}(s)=\tfrac{1}{2}[\gamma(s)+\sigma\sigma'\gamma_v(s)]. \tag{50}$$

For subscripts (σ, σ) in Eq. (50) the given point and its neighbors have the same vorticity, while $(\sigma, -\sigma)$ refers to the opposite case. Therefore a knowledge of the correlation functions $G(s)$ and $G_v(s)$ that are calculated in Appendix [formulas (A6) and (A24)] is enough to find the chiral mean densities and correlation functions. These chirality-dependent correlation functions are shown graphically in Fig. 5 in the scaled form

$$g_{\sigma\sigma'}(\ell)=\frac{\gamma_{\sigma\sigma'}(\ell/\sqrt{\rho})}{\rho}. \tag{51}$$

Also in this case we find good agreement with Berry and Dennis [18]. Above we alluded to the general shape of pair correlation functions for amorphous materials. With the dependence on σ included we may obviously carry this naive picture a bit further to talk in a loose way about the nodal points as a two-component system in which ''objects'' with the same vorticities (topological charges) repel each other. At the same time ''objects'' with opposite σ may approach each other closely. Hence we may think about the system of nodal points as a thin slab of a fictitious binary amorphous solid or salt [28]. Of course, this analogy should not be pushed too far.

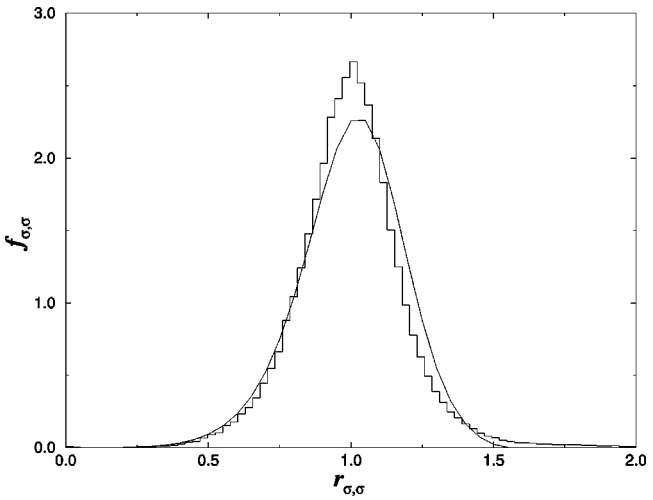

FIG. 6. Distribution functions of nearest distances between nodal points with the same chirality σ versus dimensionless distance (33) with $\langle\ell\rangle=0.998$. Solid line is calculated from function (53). The histogram refers to numerical work as described in Fig. 2. For this case we obtain the same value for $\langle\ell\rangle$.

In order to find the distributions functions $f_{\sigma\sigma'}(\ell)$ for nearest distances between nodal points with chiralities σ and σ' we insert $g_{\sigma\sigma'}(\ell)$ into Eq. (31). For the Bernoulli approximation one also has to label the mean number of points (38) as

$$\langle n_{\sigma,\sigma'}(\ell)\rangle=2\pi\int_0^\ell g_{\sigma,\sigma'}(z)z\,dz, \tag{52}$$

which is to be inserted in Eq. (41). We have found above, however, that already the Poisson approximation catches the gross features of the nearest neighbor distribution. For this reason and because the Bernoulli approximation is very tedious we will restrict ourselves to the Poisson approximation at this stage. Thus we consider

$$f_{\sigma\sigma'}(\ell)=2\pi\ell g_{\sigma\sigma'}(\ell)\exp\left[-2\pi\int_0^\ell z g_{\sigma\sigma'}(z)\,dz\right]. \tag{53}$$

Using Eqs. (50), (52), and (53) one can show that the asymptote of $f_{\sigma,-\sigma}(\ell)$ coincides with the asymptote for the DFNDNP (29). For $f_{\sigma,\sigma}(\ell)$, however, we obtain the quite different form

$$f_{\sigma,\sigma'}(\ell)=\frac{5\pi}{81}\sqrt{10\pi}\ell^4\approx 1.09\ell^4. \tag{54}$$

The σ-dependent DFNDNP (53) for (σ, σ) and $(\sigma, -\sigma)$ are compared with numerical results in Figs. 6 and 7. The difference between the two combinations (σ, σ) and $(\sigma, -\sigma)$ is very clear. In the first case there is a strong repulsion between the nearest neighbors, a result that is to be expected from Fig. 5. The distribution is, however, of a very simple form. Essentially it corresponds a symmetric ring (first shell)

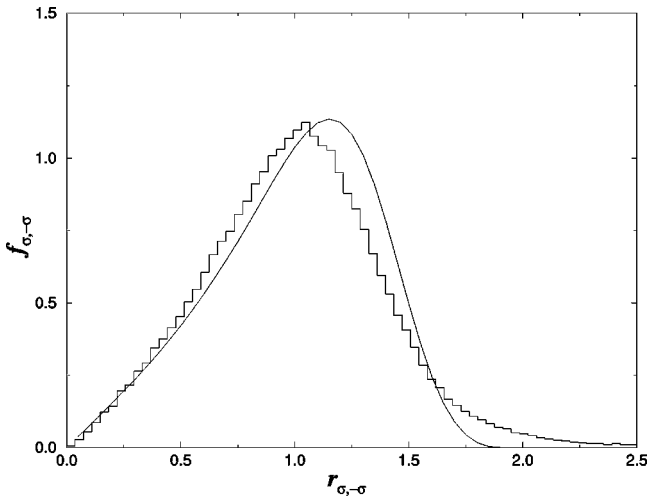

FIG. 7. Same as in Fig. 6 but for nodal points with opposite chiralities σ; $\langle \mathcal{C} \rangle = 0.696$. The histogram refers to numerical work as described in Fig. 2. For this case we find $\langle \mathcal{C} \rangle = 0.726$.

around the given point. Except for the low tail regions it is well approximated by a Gaussian, i.e., there is basically a random distribution within the ''shell.''

In the second case $(\sigma, -\sigma)$, the distribution shows how the nodal points are allowed to come arbitrarily close to each other and how the shell structure is less pronounced. For small separations $f_{\sigma,-\sigma}$ is obviously the dominant term in the total distribution f. Finally we note that $\langle \mathcal{C} \rangle \simeq 0.7$ for opposite chiralities (topological charges) and $\langle \mathcal{C} \rangle \simeq 1$ for equal chiralities, i.e., there are ''inner'' and ''outer shells'' for opposite and equal vorticities, respectively. As shown by Figs. 6 and 7 the Poisson approximation reproduces the numerical results in at least a qualitatively correct way.

VI. SUMMARY

We have considered the distribution among nodal points associated with chaotic wave dynamics. The nodal points are of special interest as they are associated with vortical flow and chirality σ that is either $+1$ or -1. In particular we have focused on the distribution of nearest separations among the nodal points. The reason is that distributions of this kind may carry information about chaotic dynamics as conjectured in [10]. We have introduced analytic approaches based on complex Gaussian random functions with the known correlation function $J_0(ks)$. Two cases have been considered, namely, the Poisson and Bernoulli approximations.

As a supplement to the analytic approaches we have performed numerical calculations to locate the nodal points and their vorticity using the Berry chaotic wave function in Eq. (1). The numerical distributions computed in this way are, in principle, the correct ones and are therefore useful for testing the accuracy of the analytic modeling. We thus find that already the Poisson approximation gives a good qualitative understanding of the distribution of nearest neighbor separations. Some higher-order correlations are, however, not accounted for. For this reason we have also considered the Bernoulli approximation that picks up some of these features. On the other hand the behavior at large distances needs further work.

When the distribution of nearest neighbor distances is separated into distances between nodal points with equal and opposite chiralities one obtains a picture that superficially reminds of binary amorphous matter. There are distinct ''inner'' and ''outer shells'' associated with opposite and equal chiralities, respectively. While points with opposite chiralities may get close to each other there is a strong repulsion among pairs with equal chirality. The reason is, loosely speaking, that nodal points with equal chirality have to appear in conjunction with ''antivortices'' or saddle points. These ''antivortices'' act as local ''beam splitters'' and are necessary for two nearby vortices to spin the same way. These interesting features should be pursued further because the distributions among the different phase singularities are obviously interrelated. Effectively we may then arrive at a description reminding of a ternary amorpous materials.

The distributions discussed here relate to generic features of a wave-chaotic state. For this reason it would be of interest if they could be verified experimentally. Using, e.g., microwave cavities this appears to be a real possibility [17].

ACKNOWLEDGMENTS

This work was supported by the Swedish Institute (A.I.S.), the Royal Swedish Academy of Sciences (A.F.S.), Russian Foundation for Basic Research (A.F.S., Grant No. 01-02-16077), and the Swedish Natural Science Research Council. We are also grateful to Michael Berry and Mark Dennis for discussions and for making Refs. [18] and [19] available to us before publication. The problem of the statistical properties of vortices in 2D is somewhat esoteric and has remained dormant for many years. It is therefore surprising that we have worked in parallel on this problem.

APPENDIX: CORRELATION FUNCTIONS FOR THE NODAL POINTS

In this appendix we outline the somewhat tedious derivation of the various correlation functions. Consider the correlation function of the random density (13)

$$G(s) = \langle |\omega(\mathbf{r})\omega(\mathbf{r}+\mathbf{s})| \delta(u(\mathbf{r}))\delta(u(\mathbf{r}+\mathbf{s}))\delta(v(\mathbf{r}))\delta(v(\mathbf{r}+\mathbf{s}))\rangle. \tag{A1}$$

Since u and v are statistically independent random fields it is sufficient to consider only the statistical properties of field u. First of all, note that the joint distribution of the values of the scalar Gaussian random field at the points $\mathbf{r}$ and $\mathbf{r}+\mathbf{s}$ has the form

$$W(u,u_s) = \langle \delta(u(\mathbf{r})-u)\delta(u(\mathbf{r}+\mathbf{s})-u_s)\rangle = \frac{1}{2\pi\sqrt{1-a^2(s)}} \exp\left[-\frac{u^2+u_s^2-2a(s)uu_s}{2[1-a^2(s)]}\right]. \tag{A2}$$

Furthermore, we will need the reciprocal statistical properties

of Gaussian scalar field u and its gradient ∇u. They are completely defined by the correlation vector

$$\mathbf{e}(\mathbf{s})=\langle u(\mathbf{r}+\mathbf{s})\nabla u(\mathbf{r})\rangle \tag{A3}$$

and the correlation tensor $b_{ij}(\mathbf{s})$, $i,j=1,2$ of vector field ∇u.

It is convenient to project this vector and tensor onto the local coordinate system related to the vector $\mathbf{s}$ through the longitudinal components

$$u_{\parallel}(\mathbf{r}),\quad u_{\parallel}(\mathbf{r}+\mathbf{s})$$

and the transverse ones

$$u_{\perp}(\mathbf{r}),\quad u_{\perp}(\mathbf{r}+\mathbf{s}).$$

These components have the remarkable correlation properties

$$\langle u(\mathbf{r}+\mathbf{s})u_{\parallel}(\mathbf{r})\rangle=e(s),\quad \langle u(\mathbf{r}+\mathbf{s})u_{\perp}(\mathbf{r})\rangle=0. \tag{A4}$$

The tensor correlation function becomes diagonal

$$\langle u_{\parallel}(\mathbf{r})u_{\parallel}(\mathbf{r}+\mathbf{s})\rangle=b_{\parallel}(s)\quad \langle u_{\perp}(\mathbf{r})u_{\perp}(\mathbf{r}+\mathbf{s})\rangle=b_{\perp}(s), \tag{A5}$$

$$\langle u_{\parallel}(\mathbf{r})u_{\perp}(\mathbf{r}+\mathbf{s})\rangle=0.$$

Here we introduce the following notations:

$$b_{\parallel}(s)=-\frac{d^2a(s)}{ds^2},\quad b_{\perp}(s)=-\frac{1}{s}\frac{da(s)}{ds},$$

$$e(s)=-\frac{da(s)}{ds},\quad b_{\parallel}(0)=b_{\perp}(0)=\frac{1}{2}k^2=b.$$

We may then write the density correlation function (A1) as

$$G(s)=\frac{1}{4\pi^2[1-a^2(s)]}\langle|u_{\parallel}v_{\perp}-v_{\parallel}u_{\perp}||u_{\parallel s}v_{\perp s}-v_{\parallel s}u_{\perp s}|\rangle. \tag{A6}$$

For brevity we have written here the dependence on s as an index. The following averages are performed for the eight manifold Gaussian fields

$$\{u_{\parallel}(\mathbf{r}),u_{\parallel}(\mathbf{r}+\mathbf{s})\},\quad \{v_{\parallel}(\mathbf{r}),v_{\parallel}(\mathbf{r}+\mathbf{s})\},$$

$$\{u_{\perp}(\mathbf{r}),u_{\perp}(\mathbf{r}+\mathbf{s})\},\quad \{v_{\perp}(\mathbf{r}),v_{\perp}(\mathbf{r}+\mathbf{s})\}. \tag{A7}$$

Here each pair of variables has the correlation properties

$$\langle u_{\parallel}^2\rangle=\langle v_{\parallel}^2\rangle=b\Delta(s),$$

$$\langle u_{\perp}^2\rangle=\langle v_{\perp}^2\rangle=b,$$

$$\langle u_{\parallel}u_{\parallel s}\rangle=\langle v_{\parallel}v_{\parallel s}\rangle=c(s),$$

$$\langle u_{\perp}u_{\perp s}\rangle=\langle v_{\perp}v_{\perp s}\rangle=b_{\perp}(s), \tag{A8}$$

where

$$\Delta(s)=\frac{b[1-a^2(s)]-e^2(s)}{b[1-a^2(s)]},$$

$$c(s)=\frac{b_{\parallel}(s)[1-a^2(s)]-a(s)e^2(s)}{b[1-a^2(s)]}. \tag{A9}$$

It is convenient to transform to normalized random variables

$$\tilde{u}_{\parallel}=\frac{u_{\parallel}}{\sqrt{b\Delta(s)}},\quad \tilde{v}_{\parallel}=\frac{v_{\parallel}}{\sqrt{b\Delta(s)}},\quad \tilde{u}_{\perp}=\frac{u_{\perp}}{\sqrt{b}},\quad \tilde{v}_{\perp}=\frac{v_{\perp}}{\sqrt{b}}.$$

With the correlation coefficients

$$\alpha=\frac{b_{\parallel}(s)[1-a^2(s)]-a(s)e^2(s)}{b[1-a^2(s)]-e^2(s)},\quad \beta=\frac{b_{\perp}(s)}{b} \tag{A10}$$

expression (A6) now takes the form

$$G(s)=\rho^2\frac{\Delta(s)}{1-a^2(s)}\Lambda(\alpha,\beta), \tag{A11}$$

where

$$\Lambda(\alpha,\beta)=\langle|\tilde{u}_{\parallel}\tilde{v}_{\perp}-\tilde{v}_{\parallel}\tilde{u}_{\perp}||\tilde{u}_{\parallel s}\tilde{v}_{\perp s}-\tilde{v}_{\parallel s}\tilde{u}_{\perp s}|\rangle \tag{A12}$$

and the averaging is performed with respect to the distributions

$$w_{\parallel}(u,u_s)=\frac{1}{2\pi\sqrt{1-\alpha^2}}\exp\left[-\frac{u^2+u_s^2-2\alpha uu_s}{2(1-\alpha^2)}\right]$$

$$w_{\perp}(u,u_s)=\frac{1}{2\pi\sqrt{1-\beta^2}}\exp\left[-\frac{u^2+u_s^2-2\beta uu_s}{2(1-\beta^2)}\right].$$

Here distribution $w_{\parallel}$ describes the statistics of ''parallel pairs'' $\{u_{\parallel},u_{\parallel s}\}$ and $\{v_{\parallel},v_{\parallel s}\}$ while $w_{\perp}$ describes properties of ''perpendicular'' ones.

It remains to calculate the function (A12) that will be done in two steps. First, we average over the statistical ensemble of parallel components $\{u_{\parallel},u_{\parallel s},v_{\parallel},u_{\parallel s}\}$ at all given perpendicular variables to obtain

$$\Lambda_{\perp}(\alpha,\beta)=\langle|\lambda\lambda_s|\rangle_{\perp}, \tag{A13}$$

where notation $\langle\cdots\rangle_{\perp}$ means that all perpendicular variables are considered as fixed, and that

$$\lambda=\tilde{u}_{\parallel}\tilde{v}_{\perp}-\tilde{u}_{\parallel}\tilde{v}_{\perp},\quad \lambda_s=\tilde{u}_{\parallel s}\tilde{v}_{\perp s}-\tilde{v}_{\parallel s}\tilde{u}_{\perp s}$$

are two Gaussian variables with zero mean values with dispersions

$$\langle\lambda_{\perp}^2\rangle=\tilde{u}_{\perp}^2+\tilde{v}_{\perp}^2,\quad \langle\lambda_{\perp s}^2\rangle=\tilde{u}_{\perp s}^2+\tilde{v}_{\perp s}^2$$

and correlation

$$\langle\lambda\lambda_s\rangle_{\perp}=\alpha(\tilde{u}_{\perp}\tilde{u}_{\perp s}+\tilde{v}_{\perp}\tilde{v}_{\perp s}).$$

Let us normalize variables λ and λ_s by the relations

$$z=\frac{\lambda}{\sqrt{u_{\perp}^2+v_{\perp}^2}},\quad z_s=\frac{\lambda_s}{\sqrt{u_{\perp s}^2+v_{\perp s}^2}},$$

which transform the function (A13) as

$$\Lambda_\perp(\alpha,\beta)=\sqrt{(u_\perp^2+v_\perp^2)(u_{\perp s}^2+v_{\perp s}^2)}\langle|zz_s|\rangle_\perp, \quad \text{(A14)}$$

where z and z_s are Gaussian variables with unit dispersion and the correlation coefficient as

$$\gamma=\langle zz_s\rangle_\perp=\alpha\frac{u_\perp u_{\perp s}+v_\perp v_{\perp s}}{\sqrt{(u_\perp^2+v_\perp^2)(u_{\perp s}^2+v_{\perp s}^2)}}.$$

Using the properties of Gaussian random variables one can derive, after some algebra, the following equation:

$$\frac{d^2\langle|z_1z_2|\rangle_\perp}{d\gamma^2}=4\langle\delta(z_1)\delta(z_2)\rangle_\perp=\frac{2}{\pi\sqrt{1-\gamma^2}}. \quad \text{(A15)}$$

Taking into account the initial conditions

$$\langle|z_1z_2|\rangle_\perp|_{\gamma=0}=\frac{2}{\pi}, \quad \frac{d\langle|z_1z_2|\rangle_\perp}{d\gamma}|_{\gamma=0}=0,$$

we obtain from Eq. (A15)

$$\mathcal{F}(\gamma)=\langle|zz_s|\rangle_\perp=\frac{2}{\pi}[\sqrt{1-\gamma^2}+\gamma\arcsin\gamma]. \quad \text{(A16)}$$

Substituting Eq. (A16) in Eq. (A14) and averaging over the remaining four perpendicular random variables we obtain

$$\Lambda(\alpha,\beta)=\langle\Lambda_\perp(\alpha,\beta)\rangle=\langle\sqrt{(u_\perp^2+v_\perp^2)(u_{\perp s}^2+v_{\perp s}^2)}\mathcal{F}(\gamma)\rangle. \quad \text{(A17)}$$

The angular brackets on the right hand of this equation imply an averaging over the $\perp$ variables with the following joint distribution

$$w(u,u_s,v,v_s)=\frac{1}{4\pi^2(1-\beta^2)}\times\exp\left[-\frac{u^2+v^2+u_s^2+v_s^2-2\beta(uu_s+vv_s)}{2(1-\beta^2)}\right].$$

In order to perform integration over four $\perp$ variables $\{u,u_s,v,v_s\}$ we use the polar system of coordinates

$$u_\perp=\xi\cos\varphi, \quad v_\perp=\xi\sin\varphi \quad u_{\perp s}=n\cos\psi, \quad v_{\perp s}=n\sin\psi,$$

which gives, instead of Eq. (A17),

$$\Lambda(\alpha,\beta)=\langle\xi\eta\mathcal{F}(\alpha\cos\mu)\rangle \quad (\mu=\varphi-\psi). \quad \text{(A18)}$$

Here the three random variables $\{\xi,\ \eta,\ \mu\}$ are distributed as

$$w(\xi,\eta,\mu)=\frac{\xi\eta}{2\pi(1-\beta^2)}\exp\left[-\frac{\xi^2+\eta^2-2\beta\xi\eta\cos\mu}{2(1-\beta^2)}\right],$$

$$\xi,\eta>0, \quad \mu\in[-\pi,\pi].$$

To exclude the random variables ξ and η we rewrite relation (A18) as

$$\Lambda(\alpha,\beta)=\frac{1}{2\pi}\int_{-\pi}^{\pi}\mathcal{F}(\alpha\cos\mu)\mathcal{A}(\mu,\beta)d\mu, \quad \text{(A19)}$$

where

$$\mathcal{A}(\mu,\beta)=\frac{1}{1-\beta^2}\times\int_0^\infty d\xi\int_0^\infty d\eta\xi^2\eta^2\times\exp\left[-\frac{\xi^2+\eta^2-2\beta\xi\eta\cos\mu}{2(1-\beta^2)}\right]. \quad \text{(A20)}$$

If we use the new variables of integration p, δ defined through

$$\xi=p\cos\delta, \quad \eta=p\sin\delta,$$

the integral (A20) transforms into the form

$$\mathcal{A}(\mu,\beta)=\tfrac{1}{8}(1-\beta^2)^2\int_0^\pi d\theta\sin^2\theta\int_0^\infty dpp^5\exp[-\tfrac{1}{2}p^2(1-\beta\cos\mu\sin\theta)]$$

with $\theta=2\delta$. After integration over p we obtain

$$\mathcal{A}(\mu,\beta)=(1-\beta^2)^2Q(\beta\cos\mu). \quad \text{(A21)}$$

$$Q(z)=\frac{3z}{(1-z^2)^2}+\frac{1+2z^2}{(1-z^2)^{5/2}}\left[\arctan\left(\frac{z}{\sqrt{1-z^2}}\right)+\frac{\pi}{2}\right]. \quad \text{(A22)}$$

Substituting Eq. (A21) in Eq. (A19) we finally obtain

$$\Lambda(\alpha,\beta)=\frac{(1-\beta^2)^2}{2\pi}\int_{-\pi}^{\pi}\mathcal{F}(\alpha\cos\mu)Q(\beta\cos\mu)d\mu, \quad \text{(A23)}$$

where the function $\mathcal{F}(\gamma)$ is defined by the equality (A16) and the function $Q(\gamma)$ is given by Eq. (A22).

For the σ-dependent density correlation functions it is easy to show, using the Gaussian properties of the fields u and v, that the correlation function for σ-dependent random density (11) has the form

$$G_v(s)=\langle R_v(\mathbf{r})R_v(\mathbf{r}+\mathbf{s})\rangle=\rho^2\frac{2\Delta(s)}{1-a^2(s)}\alpha(s)\beta(s). \quad \text{(A24)}$$

[1] S. W. McDonald and A. N. Kaufmann, Phys. Rev. Lett. **42**, 1189 (1979); Phys. Rev. A **37**, 3067 (1988).

[2] A. Bäcker and R. Schubert, J. Phys. A **32**, 4795 (1999).

[3] B. Hu, B. Li, and W. Wang, Europhys. Lett. **50**, 300 (2000).

[4] J. S. Kole, K. Michielsen, and H. De Raedt, Phys. Rev. E **63**, 016201 (2000).

[5] W. E. Bies, L. Kaplan, M. R. Haggerty, and E. J. Heller, e-print arXiv:nlin.CD/0004024.

[6] H.-J. Stöckman, *Quantum Chaos* (Cambridge University Press, Cambridge, 1999).
[7] Y. V. Fyodorov and H.-J. Sommers, J. Math. Phys. **38**, 1918 (1997).
[8] F.-M. Dittes, Habilitation thesis, Dresden Technical University, 1998.
[9] H. Ishio, Phys. Rev. E **62**, R3035 (2000).
[10] K.-F. Berggren, K. N. Pichugin, A. F. Sadreev, and A. A. Starikov, JETP Lett. **70**, 403 (1999) [Pis'ma Zh. Eksp. Teor. Fiz. **70**, 398 (1999)].
[11] P. A. M. Dirac, Proc. R. Soc. London, Ser. A **133**, 60 (1931).
[12] J. O. Hirschfelder, A. C. Christoph, and W. E. Palke, J. Chem. Phys. **61**, 5435 (1974).
[13] J. O. Hirschfelder, J. Chem. Phys. **67**, 5477 (1977).
[14] K.-F. Berggren and Z.-L. Ji, Phys. Rev. B **47**, 6390 (1993).
[15] H. Wu and D. W. L. Sprung, Phys. Lett. A **183**, 413 (1993).
[16] P. Exner, P. Šeba, A. F. Sadreev, P. Streda, and P. Feher, Phys. Rev. Lett. **80**, 1710 (1998).
[17] P. Šeba, U. Kuhl, M. Barth, and H.-J. Stöckmann, J. Phys. A **32**, 8225 (1999).
[18] M. V. Berry and M. R. Dennis, Proc. R. Soc. London, Ser. A **456**, 2059 (2000), and references therein.
[19] M. V. Berry and M. R. Dennis, Proc. R. Soc. London, Ser. A **457**, 141 (2001).
[20] J. F. Nye, *Natural Focusing of Light* (IOP, Bristol, 1999).
[21] *Optical Vortices*, edited by M. Vasnetsov and K. Staliunas (Nova, Commack, NY, 1999).
[22] M. Soskin and M. Vasnetsov, Photonics Sci. News **4**, 21 (1999).
[23] R. Blümel, I. H. Davidson, W. P. Reinhardt, H. Lin, and M. Sharnoff, Phys. Rev. A **45**, 2641 (1992).
[24] M. R. Dennis, *Second International Conference on Singular Optics (Optical Vortices): Fundamentals and Applications* (SPIE, Bellingham, Washington).
[25] B. I. Halperin, in *Physics of Defects*, edited by R. Balian, N. Kleman, and J.-P. Poirer (North Holland, Amsterdam, 1981). A general expression for the correlation function for topological defects is presented. Unfortunately there is no derivation given.
[26] M. S. Longuet-Higgins, Philos. Trans. R. Soc. London, Ser. A **249**, 321 (1957).
[27] M. S. Longuet-Higgins, J. Opt. Soc. Am. **50**, 838 (1960).
[28] For a general text on amorphous solids see, e.g., the classical work by N. F. Mott and E. A. Davis, *Electronic Processes in Non-Crystalline Materials* (Clarendon Press, Oxford, 1979).
[29] F. Haake, in *Quantum Signatures of Chaos* (Springer-Verlag, Berlin, 1991), p. 200.
[30] J. R. Eggert, Phys. Rev. B **29**, 6664 (1984).